Journal of Climate Change
ISSN 2395-7611 Volume 11 (2025) No. 4. pp. 432–449

https://doi.org/10.70917/jcc-2025-028
Article

Comparative Thermal and Electrical Performance Analysis of PV/T Collectors with Different Finned Absorber Configurations

Mahmut Sami Buker [1,2,*], Ahmet Emre Onay [3] and Halil Ibrahim Dag [4]

[1] Science and Technology Research and Application Center, Energy and Semiconductors Research Group, Necmettin Erbakan University, Konya 42090, Turkiye
[2] Faculty of Aviation and Space Sciences, Department of Aeronautical Engineering, Necmettin Erbakan University, Konya 42090, Turkiye
[3] Innorma R&D Corp, Konya 42250, Turkiye
[4] SOLIMPEKS Solar Corp, Konya 42250, Turkiye
* Correspondence author: msbuker@erbakan.edu.tr

Abstract: This study investigates and compares the thermal and electrical performance of three photovoltaic/thermal (PV/T) solar collectors with different absorber plate geometries. A standard flat-plate PV/T panel serves as the baseline, while two enhanced designs incorporate aluminium finned absorbers (with 112 and 229 fins) beneath the PV cells to increase surface area for heat dissipation via water cooling. Performance was evaluated through both computational fluid dynamics (CFD) simulations and outdoor experimental testing. Both simulated and measured results confirmed that absorber plate designs affect the efficiency of PV/T systems. The prototype featuring 229 fins delivered better thermal performance and lower PV cell operating temperatures, resulting in improved electrical output. The 112-fin variant demonstrated intermediate performance in both aspects, balancing manufacturability and effectiveness. Sustainability implications were also evaluated, with the 229-fin configuration showing a 24.48% increase in CO_2 reduction potential compared to the standard design, offering a substantial contribution to climate change mitigation. These findings underscore the potential of finned PV/T systems in enhancing both energy efficiency and environmental benefits, making them a promising option for large-scale renewable energy applications.

Keywords: hybrid photovoltaic thermal collector; absorber plate; heat transfer enhancement; electrical efficiency

1. Introduction

Photovoltaic/thermal (PV/T) systems enhance solar utilisation by combining electricity generation with thermal energy recovery. Transferring excess heat to a circulating fluid helps produce usable thermal energy and lowers PV cell temperatures, boosting electrical efficiency. Absorber plate design plays a key role, with finned absorbers enhancing heat transfer by increasing surface area and promoting heat dissipation. Fin type, number, and layout notably influence system performance.

There are several studies in literature that have reported PV temperature reductions of up to 38.6°C with corrugated fins (Unnikrishnan et al., 2024), and up to 26% improvement in thermal efficiency using perforated designs (Amrizal et al., 2024). Cylindrical fins have also shown electrical efficiency gains between 9.7% and 13.8% depending on their arrangement (M. Demir et al., 2023), while systems using nanofluids and finned geometries have reached thermal efficiencies above 78% (El Hadi Attia et al., 2024). Another study highlights how factors like mass flow rate, fin spacing, and environmental conditions further influence performance. In one case, increasing the flow rate boosted thermal efficiency by over 12% (Abdullah et al., 2020). Despite promising results from simulations and small-scale tests, there's still a need for full-size, outdoor evaluations.

Some studies reinforce the importance of enhancing thermal management in PV/T systems to improve overall efficiency. One study experimentally validated a roof-integrated PV/T collector using a polyethylene heat exchanger, achieving a temperature lift of up to 16 °C and thermal efficiencies as high as 20.25%. The findings highlight how dedicated cooling structures beneath PV modules can significantly aid in waste heat recovery and improve energy payback time—insights that align with the use of absorbers in this study to boost thermal transfer (Buker et al., 2014). Similarly, another study emphasized that PV/T configurations—especially water-based systems with advanced absorber designs—offer superior performance over conventional PV setups by leveraging improved heat extraction techniques (Allouhi et al., 2023). This review study underscores the growing trend toward integrated solutions that combine structural, thermal, and economic optimisation.

Numerous studies have examined how finned absorber plates influence the electrical performance of PV/T collectors compared to conventional flat-plate designs. For instance, (Amrizal et al., 2021) reported that a double-pass PV/T air collector using a rectangular finned absorber achieved a thermal efficiency of 73.23% and an electrical efficiency of 10.16%, outperforming its single-pass counterpart. (Rao et al., 2022) found that even a carefully optimised serpentine absorber layout can deliver thermal and electrical performance on par with more complex designs. In a CFD-based investigation, (Prasetyo, Budiana, et al., 2024) highlighted the thermal benefits of finned geometries, showing clear gains in heat transfer and overall system efficiency when compared to traditional flat-plate collectors. These findings reinforce the idea that finned absorbers can lead to improved electrical output, particularly when tailored to suit specific system configurations and conditions.

Additional studies have explored alternative absorber concepts, such as a glazed flat plate collector with a roll-bond absorber, which delivered higher thermal efficiency than the standard sheet-and-tube type (Del Col et al., 2013). (Fan et al., 2019) proposed a V-corrugated absorber for liquid-based collectors, which enhanced both optical and thermal performance while also reducing pressure loss and pumping requirements. Overall, finned designs have been shown to address common challenges in PV/T systems—such as uneven temperature distribution and excess heat buildup—by promoting more consistent cooling across the collector surface, thereby improving both thermal recovery and electrical efficiency (Diwania et al., 2020).

Another study analysed the impact of partial shading on solar panel performance in dynamic environments, demonstrating that strategic use of half-cut cells and bypass diodes can mitigate energy losses by up to 3%. Their findings, though applied to solar vehicles, underscore the importance of cell configuration and shading resilience—key considerations in the design of novel absorber plates for PV/T collectors where uniform irradiance and thermal-electrical synergy are critical (Kaneria & Reddy, 2025). In another study, they developed a transient simulation model of a solar-driven organic Rankine cycle (ORC) system without thermal storage, emphasising the role of real-time solar input and dynamic control. Their use of effectiveness–NTU-based heat exchanger modelling and scroll expander-generator coupling highlights the importance of thermal response and flow regulation under fluctuating irradiance. These findings are relevant to PV/T absorber plate design, where enhancing thermal stability and responsiveness is critical for maintaining efficient hybrid operation under variable solar conditions. The temporal stability and magnitude of the thermal output from PV/T collectors influence the design and control of coupled thermal systems such as low-temperature Organic Rankine Cycle (ORC) units or heat-driven loads. For example, ORC performance and control settings depend on inlet temperature and available thermal power; therefore, absorber plate designs that produce more stable outlet temperatures can simplify ORC control and improve part-load efficiency (Kutlu et al., 2025). Other study evaluated passive cooling strategies—natural ventilation, shading, and material selection—across five rapidly growing megacities using dynamic building energy simulation. Their findings emphasize the importance of climate-responsive envelope design and thermal mass in reducing cooling loads, particularly in hot-humid regions. While focused on commercial buildings, the study's insights into thermal behaviour, material conductivity, and solar gain mitigation are directly relevant to PV/T absorber plate design, where optimising heat transfer and minimising overheating are critical for hybrid performance (Suman et al., 2025).

A study on low-cost modifications to improve PV/T performance, demonstrated that finned absorbers could increase thermal efficiency by 30% compared to unfinned systems while simultaneously improving electrical output by 2-4%. These findings established a foundation for subsequent research on finned PV/T systems (Tonui & Tripanagnostopoulos, 2007). Another study investigated the impact of fin spacing and height on overall PV/T performance. The mathematical model, validated through indoor experiments, indicated an optimal fin spacing of 10-12 mm for water-based PV/T systems, with diminishing returns observed for fin heights above 25 mm. The experimental validation showed agreement within 8% of theoretical predictions (Yang & Athienitis, 2012). In another study, a finned and unfinned PV/T collector has been comparably analysed. Based on this study, fins in the system causes

PV layer temperature to reduce with the help of increased heat transfer area between the collector and the working fluid. Water/Al2O3, at 0.6 % concentration as working fluid, shows the highest electrical energy conversion rates at 13.39 %. Fins also improve thermal performance based on the working fluid used. The use of fins enhances the heat transfer flow in the fluid (Prasetyo, Arifin, et al., 2024). Researchers from the University of Technology-Iraq conducted an experimental study to enhance PV/T system performance through modified collector design featuring spherical bulges (25 mm radius in an 8 × 15 matrix). Comparing a water-cooled modified panel (at flow rates of 1.5-3.5 l/min) against an unmodified reference panel, results demonstrated notable improvements: 8.08% increase in thermal efficiency, 8.1% increase in electrical efficiency, and up to 15.4% decrease in surface temperature at the highest flow rate (3.5 L/min). The study confirms that geometric modifications to collector surfaces can significantly improve PV/T system performance through enhanced heat transfer (Ajel et al., 2023). Table 1 summarises the recent studies on finned absorber structures on PV/T systems.

Table 1. Recent studies on finned absorber structures on PV/T systems.

Study	Efficiency	PV Cell Temperature
(Alshibil et al., 2023)	7.6% electrical, 66.17% thermal	Up to 19.2°C lower than standard PV unit
(Unnikrishnan et al., 2024)	22.27%	Up to 38.6°C drops
(Gomaa et al., 2022)	-	30.8°C of temperature drop
(Prasetyo et al., 2023)	11.74% electrical 68.79% thermal efficiency	29.65°C
(K. S. et al., 2024)	49% efficiency increase	59°C temperature drop
(Qing et al., 2025)	Electrical efficiency: 8.0%, overall efficiency: 79.8%	Highest temperature drop is 11.20°C
(Göksu, 2024)	Maximum thermal efficiency reached 59.35%. Maximum electrical efficiency of exergy was 13.77%.	Maximum PV/T surface temperature: 320.437 K. Minimum PV/T surface temperature: 307.929 K.
(Souissi et al., 2024)	46.35% thermal efficiency. 13.91% electrical performance.	The lowest panel temperature is 55 °C
(Farzan et al., 2024) (Aydın et al., 2022)	Perforated baffles improve efficiency by 39.78% at 0.17 kg/s. Efficiency increases: 39.77%	Perforated baffles reduce PV temperature by 15.6% and 17.5%. Highest panel temperature drop: 17.3 °C

Consequently, the main objective of this study is to compare the performance of three PV/T collectors with different absorber designs including a standard flat plate and two finned versions with 112 and 229 fins to figure out the impact of absorber design on the performance and decide the best option. The performance assessment is performed using both CFD simulations and outdoor experiments. Therefore, the study's originality lies in its combined numerical (CFD) and full-scale outdoor experimental comparative analysis of specific fin densities (112 and 229 fins against a flat plate). This direct comparison across varied fin configurations, validated by outdoor testing data, adds to the empirical evidence in the field. The goal is to understand how absorber geometry affects thermal and electrical efficiency under practical operating conditions.

2. Material and Method

This study compares three PV/T absorber designs— a standard flat plate and two finned versions with 112 and 229 aluminium fins—using simulations and outdoor tests. In all cases, the absorber sits beneath the PV layer and is paired with water-cooled copper pipes to regulate cell temperature.

Simulations were conducted in SolidWorks Flow Simulation under standard conditions (1000 W/m² irradiance, 0.03 kg/s flow rate). Thermal performance was assessed via outlet temperature, and electrical output via cell temperature using a temperature-based efficiency model. Verified material properties and accurate boundary conditions ensured realistic results.

To validate the simulations, full-scale outdoor tests were conducted on the same three PV/T collectors. Mounted on a south-facing open-air test bench, they allowed direct comparison under similar conditions. Water was circulated through each collector via a dedicated pump and DN16 flexible piping, with inlet temperature and flow rate matching the CFD study. A buffer tank and automatic refill system ensured

stable operation by compensating for evaporation losses.

Each prototype was fitted with four sensors to measure outlet water, PV surface, and top/bottom temperatures, along with solar radiation, inlet temperature, and electrical output. A multichannel data logger recorded data every five seconds. Electrical output was regulated via a resistive load and DC power unit for realistic performance testing.

Combining simulations with outdoor tests provided a clearer understanding of how absorber geometry influences PV/T performance and validated the numerical predictions.

2.1. Description of the PV/T Systems

The 112- and 229-fin designs were chosen to assess the impact of fin density on performance. Greater fin count was expected to improve heat dissipation, lower PV temperatures, and boost efficiency—an outcome confirmed by outdoor testing. All three collectors share identical dimensions and materials, differing only in absorber plate geometry. As shown in Figure 1a, each panel consists of 3.2 mm low-iron AR-coated tempered glass, a 0.1 mm monocrystalline silicon PV layer, 1 mm EVA, and a 0.5 mm Tedlar backsheet. Beneath this, a 0.3 mm absorber plate is laminated and coupled with 8 mm copper pipes. The rear is insulated with 7.5 mm glass wool and enclosed in an aluminium casing. The finned versions (Figure 1b and Figure 1c) retain the same structure but include added internal surface area from the fins.

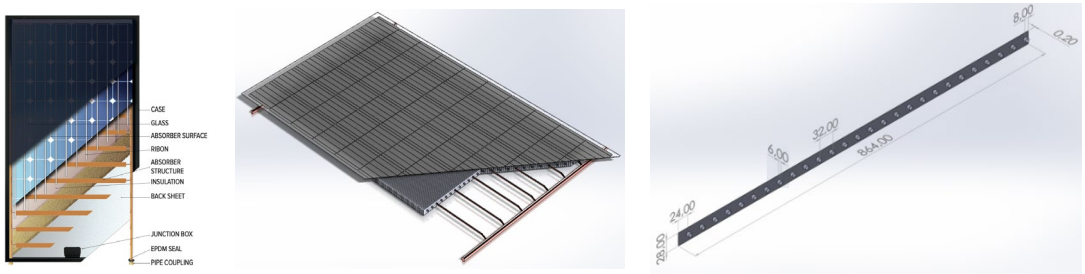

a b c

Figure 1. (**a**) PV/T collector with standard absorber (**b**) Finned absorber (**c**) Fin dimensions.

Technical specifications, including thermal conductivity, density, and optical properties of all materials used in the construction of the collectors, are listed in Tables 2, 3, 4 and 5, respectively.

Table 2. Technical specifications of the components.

Component	Parameter	Value	Units
Glass cover	Area	1.60	m^2
	Thickness	3.2	mm
	Emissivity	0.84	
	Absorptivity	0.04	
	Transmissivity	0.92	
	Reflectivity	0.04	
	Refractive Index	1.4313	
PV cells	Area of each cell	0.025	m^2
	Thickness	0.11	mm
Copper manifold tubes	Diameter	18	mm
	Number	2	
Copper collection tubes	Diameter	8	mm
	Number	7	
Tedlar	Thickness	0.5	mm
Absorber	Thickness	0.3	mm
Glasswool	Thickness	7.5	mm
Fins	Height	28	mm
	Length	864	mm
	Thickness	0.12	mm
	Spacing	12	mm

Table 3. Thermal specifications of materials.

	Thermal conductivity (W/m.K)	Specific heat (J/kg.K)	Density (kg/m^3)
Low iron tempered glass	1.8	500	3000
PV cell	148	677	2330
Tedlar	0.15	1250	1200
Eva	0.311	2090	2330
Glass wool	0,04	13000	20
Aluminium	202.4	871	2719
Copper	387.6	381	8978

Table 4. Optical properties of materials (For 500 nm wavelength) (RefractiveIndex.INFO - Refractive Index Database, n.d.).

Component	**Absorption coefficient ($1/cm^{-1}$)**	**Refractive Index**
Glass cover	0.053533	1.5103
PV cell	17700	4.2992
Aluminium	1.5200e6	0.8125
Copper	6.4622e+5	1.2134
Water	0.00025133	1.3350

Table 5. Radiative specifications of materials.

Material	**Absorbance**	**Emissivity**
Low iron tempered glass	0.04	0.84
PV cell	0.88	0.86
Tedlar	0.13	0.86
Absorber	0.95	0.05
Copper	0.18	0.05
Water	0.45	0.96
Aluminium	0.1	0.18

2.2. Numerical Simulation

The thermal and electrical performance of the PV/T collectors was modelled using SolidWorks Flow Simulation, selected for its strong integration with CAD environments and its ability to handle complex geometries such as finned absorber plates. This setup allowed for quick iterations during the design process and efficient performance evaluation across multiple absorber configurations. Its compatibility with 3D models made it particularly suited for analysing the detailed surface features introduced by the fin structures.

SolidWorks Flow Simulation solves the same fundamental Navier-Stokes equations as other industry-standard tools and is well-regarded for its reliability in thermal and fluid flow simulations. Its accuracy, when validated against experimental benchmarks, has been demonstrated in multiple prior studies.

The numerical models were configured to replicate standard test conditions used for PV/T systems, with simulations performed at a constant solar irradiance of 1000 W/m² and a mass flow rate of 0.03 kg/s, in line with Eurofins collector testing protocols. The key simulation outputs included outlet water temperature and PV cell surface temperature, which were used to estimate thermal and electrical performance under steady-state operation.

To build the simulation environment and simplify the process, several assumptions were considered as follows. The system was modelled under steady-state conditions. Solar radiation was perpendicular to the collector surface. Radiative properties were constant (gray body assumption). Absorptivity was taken equal to diffusivity for component interactions. Flow was laminar in the fluid domain. Very thin layers, such as PV cells and copper pipes, were modelled using shell conduction. Copper pipes were in good thermal contact with the absorber plate, both convection and radiation heat transfer mechanism took place in the boundary conditions, and optical properties were fixed at a wavelength of 500 nm.

To justify the laminar flow selection, Reynolds number has been calculated. The calculation parameters are as follows; total mass flow rate ($\dot{m}_{total}$) is 0.03 kg/s, number of copper collection tubes is 7, mass flow rate per pipe ($\dot{m}_{pipe}$) is $\dot{m}_{total}$/7=0.03 kg/s/7≈0.004286 kg/s, Copper pipe diameter (D) is 8 mm, inlet water temperature for simulation is 15°C, and water dynamic viscosity (μ) at 15°C is approximately 1.1375×10^{-3} Pa·s.

The Reynolds number is calculated by using following equations.

$$Re = \frac{\rho \cdot v \cdot D}{\mu} \tag{1}$$

$$\dot{m} = \rho \cdot v \cdot A \rightarrow v = \frac{\dot{m}}{\rho \cdot A} \tag{2}$$

$$Re = \frac{\rho \cdot (\frac{\dot{m}}{\rho \cdot A}) \cdot D}{\mu} = \frac{\dot{m} \cdot D}{A \cdot \mu} = \frac{\dot{m} \cdot D}{(\frac{\pi \cdot D^2}{4}) \cdot \mu} \tag{3}$$

$$Re = \frac{4 \cdot \dot{m}_{pipe}}{\pi \cdot D \cdot \mu} \tag{4}$$

Since the calculated Reynolds number is approximately 600 ($\frac{4 \cdot ,004286\ kg/s}{\pi \cdot 0.008\ m \cdot 0.0011375\ Pa \cdot s} \approx 600$), which is well below the critical point for internal pipe flow (typically 2300 for laminar-to-turbulent transition), the laminar flow assumption is fully justified for the conditions simulated. The values for Reynolds calculation are included in Table 6.

Table 6. Fluid Flow Regime Analysis (Reynolds Number Calculation).

Parameter	Value	Unit
Total Mass Flow Rate ($\dot{m}_{total}$)	0.03	kg/s
Number of Pipes	7	-
Mass Flow Rate per Pipe ($\dot{m}_{pipe}$)	0.004286	kg/s
Copper Pipe Diameter (D)	0.008	m
Water Dynamic Viscosity (μ) at 15°C	1.1375×10^{-3}	Pa·s
Calculated Reynolds Number (Re)	~600	-
Flow Regime	Laminar	-

The mesh used in the simulations consisted of 13.6 million elements and over 5 million nodes shown in Figure 2, with quality metrics kept within acceptable limits (skewness < 0.85, orthogonal quality ≈ 0.14). Thin layers like the EVA and PV layers were modelled virtually, while other components were fully represented. The SIMPLE algorithm was employed for solving momentum and energy equations, with second-order discretization for pressure, velocity, and temperature fields, and first-order for radiative transfer (DO method). Convergence was achieved using a tolerance of 1×10^{-6} for the radiation equation and 1×10^{-8} for energy (Karaaslan & Menlik, 2021).

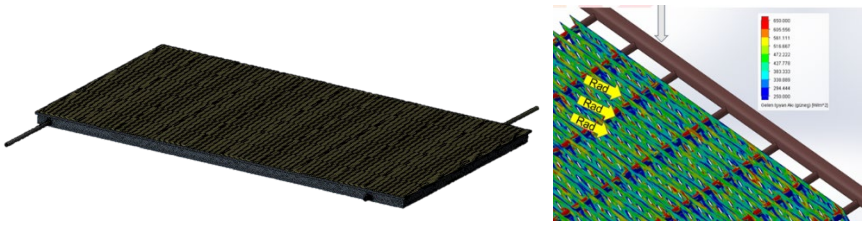

Figure 2. Meshed geometry of the standard PV/T and Finned PV/T in Flow Simulation environment.

Electrical Efficiency

Electrical efficiency was evaluated using a temperature-dependent approach based on widely accepted correlations. Under standard test conditions (1000 W/m² irradiance and reference temperature of 24,85 °C), the cell efficiency was calculated by

$$\eta_{new} = \eta_{ref}(1 - \beta_{ref}(T_{pv} - T_{ref})) \tag{5}$$

Here, η_{ref} is the reference efficiency, β_{ref} is the temperature coefficient, T_{pv} is the simulated PV cell temperature, and T_{ref} is 24,85 °C. For this study, β_{ref} was taken as 0.0041, in line with values reported in the literature for mono-crystalline PV modules. PV efficiency correlation coefficients are presented in Table 7.

Table 7. PV efficiency correlation coefficients (Dubey et al., 2013).

T_{ref} (°C)	T_{ref}	B_{ref}	Type
25	0.15	0.0041	Mono-Si
28	0.117	0.0038	Average of Sandia and commercial cells
25	0.11	0.003	Mono-Si
25	0.13	0.0041	PV/T
		0.005	PV/T
20	0.10	0.004	PV/T
25	0.10	0.0041	PV/T
20	0.125	0.004	PV/T
25		0.0026	a-Si
25	0.13	0.004	Mono-Si
	0.11	0.004	Poly-Si
	0.05	0.0011	a-Si
25	0.178	0.00375	PV/T
25	0.12	0.0045	Mono-Si
25	0.097	0.0045	PV/T
25	0.09	0.0045	PV/T
25	0.12	0.0045	PV/T
25	0.12	0.0045	PV/T
25	0.127	0.0063	PV/T
25	0.127 unglazed	0.006	PV/T
25	0.117 glazed	0.0054	PV/T

Annual Electrical Energy Yield (E_{elec})

$$E_{elec} = \eta_{PV} \times I \times A_{panel} \times H_{peak} \quad (6)$$

where η_{pv} is electrical efficiency of the PV/T panel, I is standard solar irradiance (1000 W/m² or 1 kW/m²), A_{panel} is the total panel area (1.60 m²) and H_{peak} is annual peak sun hours (1825 hours/year). The annual average global horizontal irradiance for Konya is approximately 4.6–4.8 kWh/m²/day, which corresponds directly to 4.6–4.8 peak sun hours per day—i.e., the equivalent number of hours at 1 kW/m². The value of 5 h/day (1825 h/year) is used for calculation (V. Demir, 2025).

Annual Thermal Energy Yield (E_{therm})

$$E_{therm} = \dot{m} \times c_p \times \Delta T_{water} \times H_{peak} \times 3600\ s/h/1000\ W/kW \quad (7)$$

where $\dot{m}$ is the mass flow rate (0.03 kg/s), c_p is the specific heat capacity of water (4186 J/kg°C), and ΔT_{water} is the water temperature rise (between outlet and inlet temperature).

Climate Effect

To quantify the environmental benefits, specific emission factors and embodied energy values are crucial. For grid electricity in Turkiye, an emission factor of 0.543 kg CO_2e/kWh is used. For thermal energy, a widely accepted average value for natural gas combustion, 0.2 kg CO_2/$kWh_{thermal}$, is assumed for the purpose of quantifying CO_2 reduction from displaced heat.

Annual CO_2 Reduction (CO_{2red}) Potential

$$CO_{2red} = (E_{elec} \times EF_{elec}) + (E_{therm} \times EF_{therm}) \quad (8)$$

where EF_{elec} is Electricity emission factor (0.543 kg CO2e/kWh), and EF_{therm} is thermal emission factor (0.2 kg CO_2/$kWh_{thermal}$).

Energy Payback Time (EPBT)

$$EPBT = \frac{Embodied\ Energy_{panel}}{E_{total,annual}} \quad (9)$$

where $Embodied\ Energy_{panel}$ is embodied energy per panel (kWh/panel), and $E_{total,annual}$ is total annual energy yield per panel (kWh/panel/year). Estimating the embodied energy for a hybrid PV/T system is complex due to its multi-component nature. For the standard flat-plate PV/T system, a base embodied energy of 1334 kWh/m² is used. This value is derived from the literature, specifically the "macro-level" embodied energy for a rooftop PV/T system (1380 kWh/m²) with the embodied energy of the battery (46 kWh/m²) subtracted, as the current system does not include battery storage (Tiwari et al., 2007).

The total weights for each collector are for the standard collector 4.02 kg, 112-finned collector is 5.15 kg, and for 229-finned collector 6.67 kg. Using the calculated embodied energy for the standard panel (2134.4 kWh for 1.60 m² area) and its provided weight (4.02 kg), an average embodied energy per kilogram for the standard collector is derived as 2134.4 kWh/4.02 kg≈530.945 kWh/kg. This derived embodied energy per kilogram is then applied to the weights of the finned collectors to determine their respective total embodied energies, providing a consistent and data-driven approach based on the provided information.

Whole-life carbon (WLC) proxy calculations

Embodied carbon is calculated as (Rachoutis & Koubogiannis, 2016);

$$C_{emb} = E_{emb} \times EF_{mfg} \tag{10}$$

where C_{emb} is embodied CO_2 ($kgCO_2e$ per panel), E_{emb} is embodied energy used in manufacture (kWh per panel), and EF_{mfg} is the emission factor for the energy used in manufacture ($kgCO_2e$ per kWh) (EF_{mfg}=EF_{grid}).

Annual operational CO_2 reduction (displaced emissions) is calculated as (Smith et al., 2024);

$$C_{op} = E_{elec,ann} \times EF_{elec} + E_{therm,ann} \times EF_{therm} \tag{11}$$

where C_{op} is the annual avoided CO_2 emissions ($kgCO_2e$ per panel per year), $E_{elec,ann}$ is annual electrical energy produced by the panel (kWh/year), $E_{therm,ann}$ is annual thermal energy delivered by the panel (kWh/year), EF_{elec} is the electrical grid emission factor ($kgCO_2e$/kWh), and EF_{therm} is the emission factor for the displaced thermal fuel ($kgCO_2e$/kWh).

Carbon payback time is calculated as (Rachoutis & Koubogiannis, 2016);

$$T_{payback} = \frac{C_{emb}}{C_{op}} \tag{12}$$

where $T_{payback}$ is in years. This gives the time required for operational savings to offset embodied emissions.

Cumulative net CO_2 balance after N years is calculated as (Lu & Yang, 2010);

$$C_{net}(N) = N \cdot C_{op} - C_{emb} \tag{13}$$

Positive C_{net} indicates net avoided emissions over the period N years.

Energy payback time is useful to report alongside WLC (Peng et al., 2013; Zhong et al., 2017);

$$EPBT = \frac{E_{emb}}{E_{ann}} \; with \; E_{ann} = E_{elec,ann} + E_{therm,ann} \tag{14}$$

EPBT in years; E_{ann} is total annual useful energy (kWh/year).

2.3. Experimental Setup

The experimental study has been conducted in Konya, Turkiye. The location has above average solar irradiation potential compared to other cities in the country. Figure 3 presents total solar radiation potential of Konya city. The experimental setup is located near the city centre, where abundant solar radiation is available.

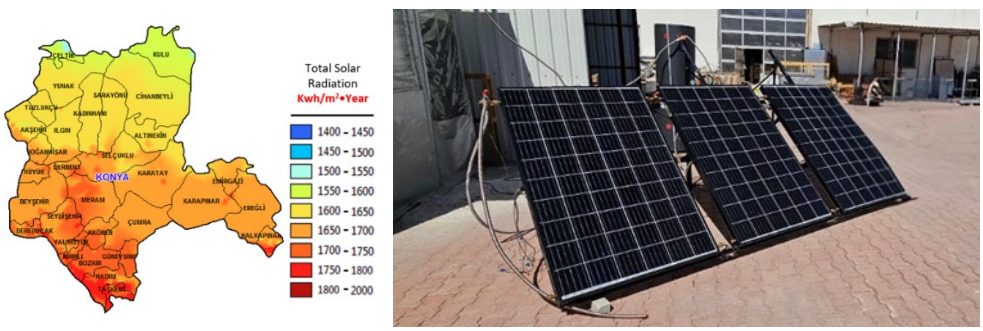

Figure 3. Total solar radiation of Konya city (GEPA - Solar Energy Potential Atlas, 2025) and experimental setup.

To experimentally validate the numerical findings, an outdoor testing rig was established using full-scale PV/T collector prototypes. The test setup was designed to ensure accurate measurement of both thermal and electrical performance under near-real operating conditions. The experiments were performed in Konya, Türkiye, and included standard as well as two types of finned absorber PV/T collectors. The test system was constructed to allow simultaneous testing of three different PV/T collectors including a standard flat-plate PV/T collector (reference), a 112-finned collector, and a 229-finned collector.

Each collector was mounted on a frame with standard tilt angles for the location to allow uniform solar exposure. Water was circulated through each collector using a parallel piping layout to ensure consistent inlet conditions. The water circulation was achieved by a pump through all three collectors. When the feed water temperature has exceeded a certain limit, it was let out by a release valve located at the top of the standard collector, then colder mains water was supplied to the system. Figure 4 presents the experimental setup diagram.

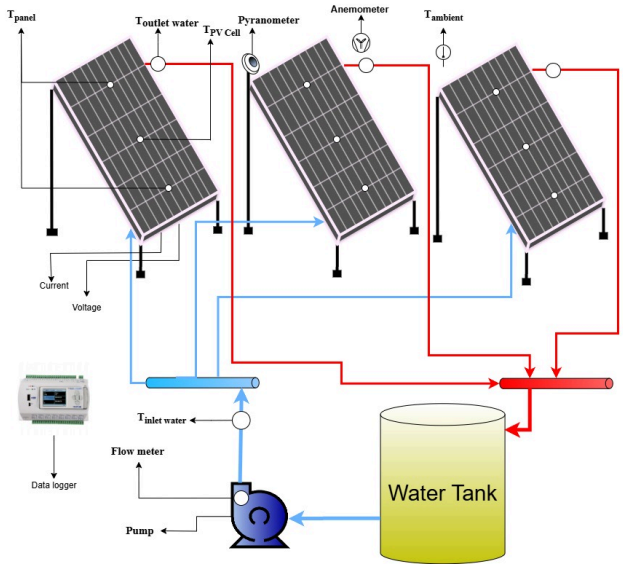

Figure 4. Experimental setup diagram.

The piping was arranged to deliver equal flow rates to all collectors using DN16 serpentine-type flexible tubing. The water flow rate and temperature were set at around 0.03 kg/s and 32.7°C during the test period. The piping system ensured hydraulic symmetry and minimised heat losses across collectors.

To enable continuous power extraction from the PV modules, each collector was connected to a DC resistive load via an inverter device. This allows the PV cells to operate under load conditions like practical use cases. Electrical power output was measured in real time using calibrated voltage and current sensors connected to each panel.

Each collector was instrumented with sensors, capturing the following parameters; irradiance (W/m²) – via a pyranometer co-located with the collectors, ambient temperature (°C) – via a temperature sensor (PT1000), inlet and outlet water temperatures (°C) – one for inlet, outlet per collector (PT1000), absorber surface temperatures – measured at top, middle, and bottom points (PT1000), and PV current and voltage (A, V) – per collector.

Data was acquired every 5 seconds using a multi-channel data logger system with a 4 GB SD card for continuous storage. To ensure system stability and avoid overheating, safety mechanisms included temperature-controlled water dumping and replenishment from the mains supply. Table 8 shows the measurement devices used in the experimental setup along with their accuracies.

Tests were performed under average mid-summer solar conditions, with solar irradiance reaching up to 881 W/m² and ambient temperatures around 30.8°C. Sky conditions were generally clear, with occasional partial cloud cover post 14:00h, as noted in irradiance fluctuation logs. The outdoor measurements reported here were performed over the mid-summer period and therefore primarily reflect warm, high-irradiance operating conditions. Seasonal variations (ambient temperature swing, wind speeds, dust deposition and winter irradiance) influence annual performance and CO_2 savings estimates. The present experimental results should be interpreted as indicative of mid-season behaviour.

Table 8. Sensors and measurement tools of the experimental setup.

Parameter	Measurement Tool	Accuracy	Range
Solar irradiance (W/m^2)	Pyranometer	±5 W/m^2	0 to 2000 W/m^2
Ambient temperature (°C)	PT1000 Temperature Sensor	±0.2°C	-50 to +500 °C
Fluid inlet/outlet temp. (°C)	PT1000 Temperature Sensor	±0.2°C	-50 to +500 °C
Water flow rate (kg/s)	Mass Flow Meter	±0.01 kg/s	0.5 to 10 m^3/s
Electrical power (V/A)	Voltage & Current Sensors	±0.1V/0.01A	0-100V / 0-10A

2.4. Results and Discussion

Simulations for all PV/T configurations were run at 1000 W/m^2 irradiance and 0.03 kg/s flow rate, with outlet temperatures shown in Table 9. A consistent temperature gradient was observed, with upper PV regions around 20% hotter than lower ones, due to the asymmetric copper pipe layout. This thermal imbalance reduced electrical efficiency by approximately 5%, as shown by the temperature-dependent model.

Table 9. Outlet water temperatures of the analysed PV/T Panels.

Panel Type	Radiation Intensity (W/m^2)	Mass flow rate (kg/s)	Inlet Temperature(°C)	Outlet Temperature(°C)
Standard	1000	0.03	15	23.98
Finned (112 Fins)	1000	0.03	15	26.62
Finned (229 Fins)	1000	0.03	15	26.85

The observed thermal non-uniformity is attributable to the present asymmetric copper pipe layout. Practical corrections include (i) adopting a symmetric header–manifold arrangement (single header with equal-spaced branch feeds or a continuous serpentine manifold with mirrored inlet/outlet positions) to reduce longitudinal temperature gradients, (ii) increasing the number of parallel collection tubes or using smaller-diameter micro-channels to lower per-pipe flow rate and improve heat extraction uniformity, and (iii) implementing hydraulic balancing elements (calibrated orifices or flow restrictors) at each feed to equalise volumetric flow. These options can be evaluated by targeted CFD optimization and prototype hydraulic testing to preserve manufacturability while improving thermal uniformity.

The temperature distribution on the PV surfaces for each configuration is visualised in Figure 5. At the given flow rate of 0.03 kg/s, the standard flat-plate collector reached maximum and minimum temperatures of 108.85 °C and 34.85 °C, respectively. The 112-fin collector performed noticeably better, with a narrower range between 65.85 °C and 32.85 °C. The 229-fin version demonstrated the most effective cooling, with a temperature span of 95.85 °C to 25.85 °C, and a large portion of its PV surface stabilized around 28.85 °C. These results clearly highlight the advantage of increasing fin density in achieving a more uniform and lower panel temperature distribution. The corresponding outlet water temperatures for the three designs were 23.98 °C (standard), 26.62 °C (112 fins), and 26.85°C (229 fins), reflecting the trend in improved thermal extraction.

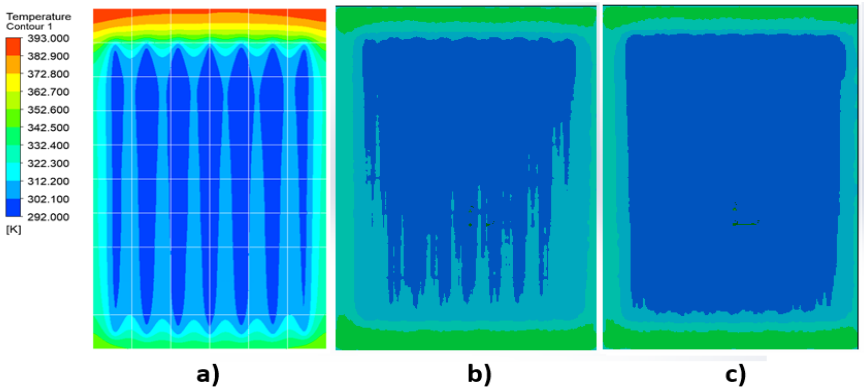

***Figure* 5.** Temperature gradient on the PV cells (under I:1000W/m_2 and ṁ: 0.03 kg/s) of a) Standard b) 112 fins c) 229 fins.

As shown in Table 10, higher fin density improved thermal management, raising outlet temperatures and lowering cell temperatures—leading to better electrical performance.

Table 10. PV cell Efficiencies based on surface temperature.

Type	η_{ref}	T_{PV}	T_{ref}	β_{ref}	η_{PV}
Standard	21.50%	66.85°C	24.85°C	0.00410	17.80%
112 fins	21.50%	46.85°C	24.85°C	0.00410	19.56%
229 fins	21.50%	38.85°C	24.85°C	0.00410	20.26%

Figure 6 illustrates natural convection heat transfer across panel layers—glass, PV cells, EVA, Tedlar, and absorber. The standard collector reached the highest temperature (66.85 °C, min. 53.85 °C), while the 229-fin and 112-fin versions peaked at 62.85 °C and 64.85 °C, with lower minimums of 24.85–25.85 °C. These results highlight the improved heat dissipation from increased surface area in finned designs. These findings support the use of higher fin densities in PV/T design, as improved cooling boosts thermal output and preserves electrical efficiency by reducing cell heat. However, increased fin count also raises panel weight, which is a drawback.

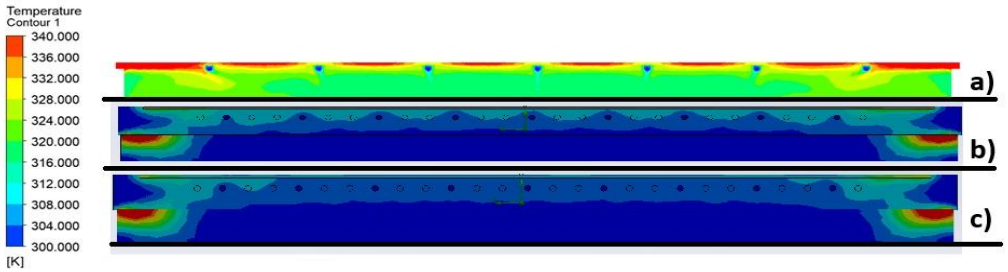

Figure 6. Temperature gradient under 1000 W/m_2 at 0.03 kg/s of mass flow rate a) Standard b) 112 fins c) 229 fins.

2.5. Experimental Validation of PV/T Collector Designs

To validate the simulations, outdoor tests were performed on the same PV/T collector types. This section compares simulation and experimental results for water temperature rise (ΔT), electrical efficiency, and PV cell temperature. Conditions followed Eurofins standards, though differences in irradiance (881 W/m² vs. 1000 W/m²) and flow rate (0.03 kg/s) affected absolute values. Therefore, emphasis is given to ΔT and relative performance.

Figure 7 shows the PV cell temperature differences for each panel. While each collector shows relatively close performance, highest temperature drop was achieved by the collector with 229 fins with a difference of 3°C compared to the standard collector. The collector with 112 fins closely follows 229 - finned collectors' performance.

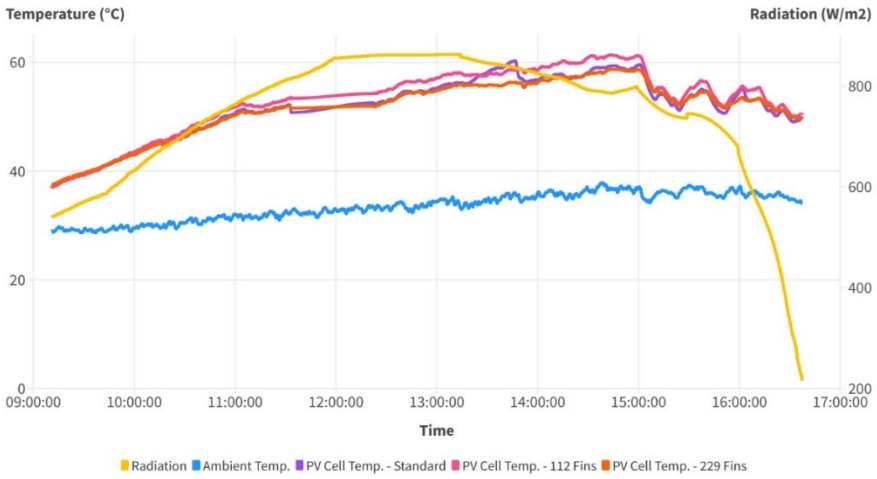

Figure 7. PV Cell temperature of each panel.

Figure 8 presents the comparison of the produced power and voltage for each collector. Due to the efficient cooling, the highest amount of power was produced by the collector with 229 fins, followed by the standard and 112 finned model. The collector with 229 fins showed better performance while the radiation dropped, at around 14:00-14:30 while other collectors dropped in performance.

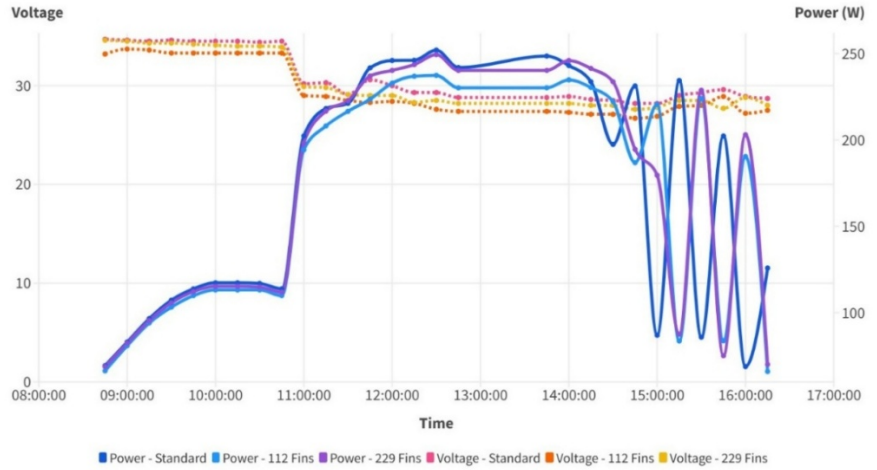

Figure 8. Electrical performances of the collectors.

The experiments showed relatively lower ΔT values due to higher inlet temperatures and system dynamics (see Table 11). However, the ranking order (229 fins > 112 fins) is preserved in both datasets.

Table 11. Comparison of experimental and simulated temperature differences.

Panel	ΔT (Simulation) [°C]	ΔT (Experiment) [°C]
Standard	9.13	8.1
112 Fins	11.77	10.6
229 Fins	12.00	11.1

Table 12 shows the simulated and experimentally obtained electrical efficiencies. Electrical efficiency was approximated from the peak electrical power output relative to irradiance. The experimental results confirm that between finned designs the 229-finned collector yield better cooling and higher electrical efficiency.

Table 12. Comparison of experimental and simulated efficiencies.

Panel	Efficiency (Simulation) [%]	Efficiency (Experiment) [%]
Standard	17.80	18
112 Fins	19.56	18
229 Fins	20.26	19

Table 13 details both simulated and experimental PV cell temperatures. While the absolute values differ, both the simulations and experiments agree on the trend that the 229-fin collector exhibits the lowest PV cell temperatures in simulation and among the lowest in practice, confirming its better thermal regulation performance.

Table 13. Comparison of experimental and simulated PV cell temperatures.

Panel	PV Temp (Simulation) [°C]	PV Temp (Experiment) [°C]
Standard	67	60.3
112 Fins	47	48.46
229 Fins	39	40.2

Finally, Figure 9 both compares simulated and experimental efficiencies and thermal differences attained through each collector. Finned designs consistently show higher electrical efficiency by maintaining lower cell temperatures. The 229-fin design leads in both simulation and experimental tests. More fins lead to greater heat transfer to the water, resulting in a higher temperature rise (ΔT) and eventually more useful thermal energy captured.

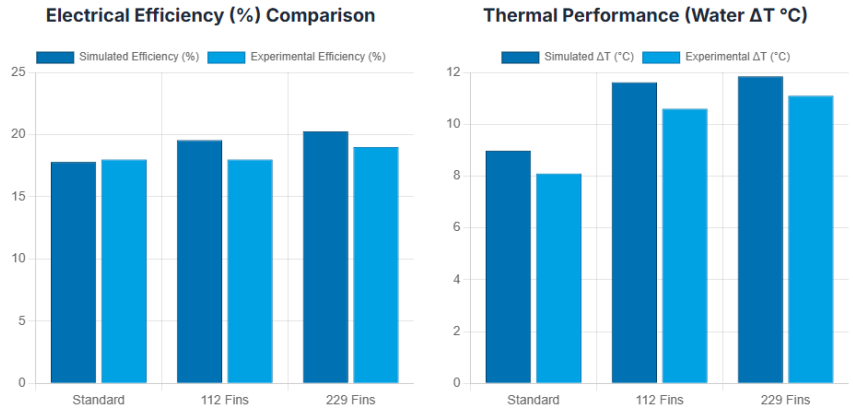

Figure 9. Efficiency and thermal performance comparison of the standard and finned PV/T collectors.

2.6. Carbon emissions reduction potential

CO_2 emission reduction analysis show that the standard panel yields 520.48 kWh electrical and 2059.8 kWh thermal energy per year (total 2580.28 kWh/year), the 112-fin panel yields 571.25 kWh electrical and 2665.4 kWh thermal energy (total 3236.65 kWh/year), and the 229-fin panel yields 591.68 kWh electrical and 2717.1 kWh thermal energy (total 3308.78 kWh/year). Using the grid emission factor of 0.543 kg CO_2e/kWh (electrical) and 0.2 kg CO_2/kWh (thermal), annual CO_2 reductions are 694.64 kg CO_2e/year (standard), 843.27 kg CO_2e/year (112 fins) and 864.65 kg CO_2e/year (229 fins), corresponding to improvements of 21.4% and 24.5% for the 112-fin and 229-fin panels relative to the standard design.. These figures quantitatively present the improved environmental benefits of the finned absorber designs (Table 14).

Table 14. Annual Energy Yields and CO_2 Savings per PV/T Panel.

Panel Type	Annual Electrical Energy (kWh/year)	Annual Thermal Energy (kWh/year)	Total Annual Energy (kWh/year)	Annual CO_2 Reduction (kg CO_2e/year)	% Improvement in CO_2 Reduction (vs. Standard)
Standard	520.48	2059.8	2580.28	694.64	-
112 fins	571.25	2665.4	3236.65	843.27	21.39%

229 fins	591.68	2717.1	3308.78	864.65	24.48%

Figure 10 presents the calculated annual cumulated energy (both thermal and electric) energy outputs. As PV/T panels generate both electricity and thermal energy, the total energy yield of the finned designs surpasses the standard collector, demonstrating better resource utilisation.

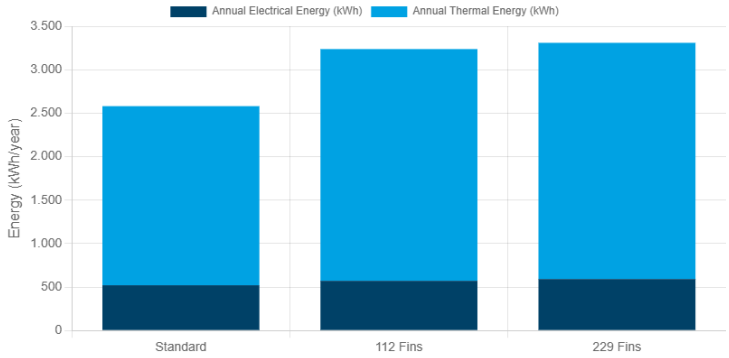

Figure 10. Annual energy production of the panels (kWh).

Although panel level environmental benefits are significant, understanding the broader implications for climate change mitigation requires extrapolating these efficiency gains to a larger deployment scale. To effectively illustrate the broader implications of these efficiency gains for climate change mitigation, the annual energy savings and CO_2 reduction are extrapolated to a hypothetical large-scale deployment scenario. A common benchmark in the solar industry, a 1 MW electrical equivalent PV/T installation, is used for this purpose. Scaling the results from a single panel to a tangible, large-scale deployment (e.g., a 1 MW electrical equivalent system) provides a powerful illustration of the technology's outdoor climate mitigation potential. This extrapolation moves beyond theoretical efficiency improvements to demonstrate practical environmental benefits at a societal or industrial level. The 229-fin configuration is selected as the optimised choice for this extrapolation due to its superior performance. Based on this approach, with 20.26% efficiency under 1000 W/m² irradiance, each 1.60 m² panel delivers 324.16 Wp. Achieving 1 MWp requires 3,085 panels over 4,936 m². Annually, the system generates ~1.83 GWh electricity, ~8.38 GWh thermal energy, and reduces ~2,668 tonnes CO_2-e.

A shorter Energy Payback Time (EPBT) indicates better energy return and sustainability. Embodied energy values are 2134.4 kWh (EPBT: 2.49 yrs) for the standard PV/T, 2734.4 kWh (EPBT: 2.55 yrs) for the 112-finned, and 3541.2 kWh (EPBT: 3.21 yrs) for the 229-finned PV/T collector. The lower EPBT of the standard panel reflects reduced material use.

The embodied-energy and energy-payback figures presented above provide a first-order comparison of the three panel configurations and support the relative operational savings reported in this work. Using the embodied-energy values reported above and the grid emission factor used elsewhere in this study (0.543 $kgCO_2e$/kWh), a preliminary conversion to embodied CO_2 yields 1,158.98 $kgCO_2e$ per panel for the standard collector, 1,484.79 $kgCO_2e$ per panel for the 112-fin design and 1,922.88 $kgCO_2e$ per panel for the 229-fin design. Dividing these embodied CO_2 values by the panels' annual operational CO_2 reductions (Table 14) gives carbon payback times of approximately 1.7, 1.8 and 2.2 years for the standard, 112-fin and 229-fin panels, respectively (Table 15). These figures are intended as a transparent, short-form WLC proxy that uses the same grid intensity assumption employed in this operational CO_2 calculations.

Table 15. Carbon Payback Calculation Results.

Panel type	**Embodied energy (kWh/panel)**	**Embodied CO_2 ($kgCO_2e$/panel)**	**Annual CO_2 reduction ($kgCO_2e$/year) (operational)**	**Carbon payback (years)**
Standard	2134.40	1,158.98	694.64	1.67
112-fin	2734.42	1,484.79	843.27	1.76
229-fin	3541.22	1,922.88	864.65	2.22

To provide a more detailed validation, the following tables present the percentage deviation and Root Mean Square Error (RMSE) for key performance metrics including water temperature rise (ΔT), electrical efficiency, and PV cell temperature. This quantitative approach allows for a clearer

understanding of the agreement and discrepancies between the numerical model and outdoor testing measurements.

While the overall trends in performance ranking (e.g., 229 fins > 112 fins > Standard for thermal performance) are largely preserved between simulation and experimental results, absolute values show varying degrees of deviation. These discrepancies can be attributed to a combination of inherent differences between idealised simulation conditions and the complexities of outdoor experiments.

Experimental ΔT values are lower than their simulated counterparts (Table 16). This is noted as being due to "higher inlet temperatures and system dynamics" during the experimental phase. The percentage deviations for electrical efficiency show mixed results (Table 17). The standard panel's experimental efficiency is slightly higher, while the finned panels show lower experimental efficiencies compared to simulation. The RMSE for PV cell temperature (4.019 °C) is notably higher than for ΔT or electrical efficiency, indicating a larger absolute difference between simulated and experimental values for this critical parameter (Table 18). The standard panel shows a lower experimental PV temperature, while finned panels show slightly higher experimental temperatures.

In summary, while the simulations effectively predict the relative performance improvements of finned designs, the absolute differences highlight the challenges of accurately modelling PV/T systems. The discrepancies underscore the importance of experimental validation to account for factors not fully captured by idealised numerical models, particularly the dynamic and variable nature of outdoor environmental conditions and the practical limitations of experimental control.

Increasing the fin density in PV/T collectors offers significant thermal and electrical performance improvements but also introduces several trade-offs. The added fins increase the overall weight of the collector, which can impact structural requirements and raise transportation and installation costs. Additionally, the material cost rises due to the higher use of aluminium and copper, while the manufacturing complexity increases with the need for advanced fabrication techniques. Fins also contribute to a higher pressure drop, which raises pumping power requirements and operational costs. Furthermore, the increased surface area may expose materials to greater thermal cycling and wear, potentially affecting long-term durability. While additional fins improve performance, beyond a certain density, diminishing returns in efficiency gains can make the added complexity and cost less justifiable. Finally, finned designs may require more frequent maintenance to prevent dirt and debris accumulation, further adding to operational costs.

Table 16. Quantitative Comparison of Water Temperature Rise (ΔT).

Panel Type	**ΔT (Simulation) [°C]**	**ΔT (Experiment) [°C]**	**Percentage Deviation (%)**
Standard	9.13	8.1	-11.28%
112 Fins	11.77	10.6	-9.94%
229 Fins	12.00	11.1	-7.50%
RMSE			**1.039 °C**

Table 17. Quantitative Comparison of Electrical Efficiency.

Panel Type	**Efficiency (Simulation) [%]**	**Efficiency (Experiment) [%]**	**Percentage Deviation (%)**
Standard	17.80	18	1.12%
112 Fins	19.56	18	-7.98%
229 Fins	20.26	19	-6.22%
RMSE			**1.164 %**

Table 18. Quantitative Comparison of PV Cell Temperature.

Panel Type	**PV Temp (Simulation) [°C]**	**PV Temp (Experiment) [°C]**	**Percentage Deviation (%)**
Standard	67	60.3	-9.99%
112 Fins	47	48.46	3.11%
229 Fins	39	40.2	3.08%
RMSE			**4.019 °C**

3. Conclusion

This study examined the thermal and electrical performance of three PV/T collector designs—a flat-plate absorber and two finned absorbers with 112 and 229 aluminium fins—using CFD simulations

alongside full-scale outdoor experiments. This combined numerical-experimental approach elucidated how absorber geometry influences PV/T efficiency under realistic operating conditions.

Experimentally, the 229-fin collector kept PV cells roughly 20 °C cooler than the flat-plate panel (about 40 °C vs 60 °C) and delivered a larger water temperature rise (~11 °C vs ~8 °C). This improved cooling translated to higher electrical output and thermal energy capture, confirming the benefits of greater fin density. The 112-fin variant showed intermediate gains between the flat and 229-fin designs, illustrating a balance between performance improvement and added complexity. Simulation results mirrored these trends but projected slightly higher efficiencies than measured, highlighting the importance of outdoor testing validation.

Beyond these performance metrics, the sustainability implications are notable. The 229-fin design yields roughly 24% more total annual energy (and CO_2 savings) per panel than the standard design. Extrapolating to a 1 MW_e array, this advanced system could annually produce around 10 GWh of combined electricity and heat, offsetting about 2,600 tonnes of CO_2. However, this performance boost slightly increases the Energy Payback Time (EPBT) due to added material: approximately 3.21 years for the 229-fin model versus ~2.50 years for the flat panel (both are only a few years, far shorter than the system lifetime). Overall, optimised finned absorbers substantially improve PV/T collector efficiency and climate benefits, underscoring their potential for large-scale deployment in renewable energy systems to help mitigate climate change.

Future work may explore alternative fin designs, materials, or hybrid cooling, along with performance under varied climates. Also, a long-term year-round test to capture seasonal performance would be considered. The findings will support the development of more efficient, durable PV/T systems for building-integrated and off-grid use.

Acknowledgment

The authors gratefully acknowledge funding from TÜBİTAK TEYDEB 1707 (Grant No. 3225044). We also extend our sincere thanks to Innorma R&D Co. and SOLIMPEKS Solar Co. for their valuable in-kind contributions.

References

Abdullah, A. L., Misha, S., Tamaldin, N., Rosli, M. A. M., & Sachit, F. A. (2020). Theoretical study and indoor experimental validation of performance of the new photovoltaic thermal solar collector (PVT) based water system. *Case Studies in Thermal Engineering*, *18*(November 2019), 100595. https://doi.org/10.1016/j.csite.2020.100595

Ajel, M. G., Gedik, E., Wahhab, H. A. A., Mahdi, L. A. A., & Chaichan, M. T. (2023). Eexperimental Investigation of Pv/T Solar Collector Efficiency With Spherical-Shaped Protrusions on the Absorber Surface. *Journal of Engineering Science and Technology*, *18*(January), 55–64.

Allouhi, A., Rehman, S., Buker, M. S., & Said, Z. (2023). Recent technical approaches for improving energy efficiency and sustainability of PV and PV-T systems: A comprehensive review. *Sustainable Energy Technologies and Assessments*, *56*(January), 103026. https://doi.org/10.1016/j.seta.2023.103026

Alshibil, A. M. A., Farkas, I., & Víg, P. (2023). Experimental performance comparison of a novel design of bi-fluid photovoltaic-thermal module using Louver fins. *Energy Reports*, *9*, 4518–4531. https://doi.org/10.1016/j.egyr.2023.03.110

Amrizal, Amrul, Akram, M. H., Yonanda, A., & Irsyad, M. (2024). Thermal Performance of Hybrid PV/T-TEC Air Collector with Perforated-Finned Absorber Plate. *Journal of Physics: Conference Series*, *2739*(1). https://doi.org/10.1088/1742-6596/2739/1/012015

Amrizal, Hidayat, Y. P., & Irsyad, M. (2021). Performance comparison of single and double pass PV/T solar collectors integrated with rectangular plate fin absorber. *IOP Conference Series: Materials Science and Engineering*, *1173*(1), 012023. https://doi.org/10.1088/1757-899x/1173/1/012023

Aydın, A., Kayri, İ., & Aydin, H. (2022). Determination of the performance improvement of a PV/T hybrid system with a novel inner plate-finned collective cooling with Al2O3 nanofluid. *Energy Sources, Part A: Recovery, Utilization and Environmental Effects*, *44*(4), 9663–9681. https://doi.org/10.1080/15567036.2022.2136801

Buker, M. S., Mempouo, B., & Riffat, S. B. (2014). Performance evaluation and techno-economic analysis of a novel building integrated PV/T roof collector: An experimental validation. *Energy and Buildings*, *76*, 164–175. https://doi.org/10.1016/j.enbuild.2014.02.078

Del Col, D., Padovan, A., Bortolato, M., Dai Prè, M., & Zambolin, E. (2013). Thermal performance of flat plate solar collectors with sheet-and-tube and roll-bond absorbers. *Energy*, *58*, 258–269.

https://doi.org/10.1016/j.energy.2013.05.058
Demir, M., Ömeroğlu, G., & Özakin, A. N. (2023). experimental determination of the effect of fins of different cylindrical geometries on electrical and thermal efficiency in an air-cooled pvt system. *Heat Transfer Research*, *54*(3), 1–16. https://doi.org/10.1615/HEATTRANSRES.2022044259
Demir, V. (2025). Evaluation of Solar Radiation Prediction Models Using AI: A Performance Comparison in the High-Potential Region of Konya, Türkiye. *Atmosphere*, *16*(4). https://doi.org/10.3390/atmos16040398
Diwania, S., Agrawal, S., Siddiqui, A. S., & Singh, S. (2020). Photovoltaic–thermal (PV/T) technology: a comprehensive review on applications and its advancement. *International Journal of Energy and Environmental Engineering*, *11*(1), 33–54. https://doi.org/10.1007/s40095-019-00327-y
Dubey, S., Sarvaiya, J. N., & Seshadri, B. (2013). Temperature dependent photovoltaic (PV) efficiency and its effect on PV production in the world - A review. *Energy Procedia*, *33*, 311–321. https://doi.org/10.1016/j.egypro.2013.05.072
El Hadi Attia, M., Zayed, M. E., Kabeel, A. E., Khelifa, A., Irshad, K., & Rehman, S. (2024). Numerical analysis and design of a novel solar photovoltaic thermal system using finned cooling channel structures embedded with air/TiO2–water nano bi-fluid. *Solar Energy*, *269*(January), 112368. https://doi.org/10.1016/j.solener.2024.112368
Fan, M., You, S., Gao, X., Zhang, H., Li, B., Zheng, W., Sun, L., & Zhou, T. (2019). A comparative study on the performance of liquid flat-plate solar collector with a new V-corrugated absorber. *Energy Conversion and Management*, *184*(January), 235–248. https://doi.org/10.1016/j.enconman.2019.01.044
Farzan, H., Iranmanesh, A., & Mohsenifard, A. (2024). Investigation on different cooling strategies for photovoltaic thermal Systems: An experimental study. *Applied Thermal Engineering*, *250*, 123537. https://doi.org/10.1016/J.APPLTHERMALENG.2024.123537
GEPA - Solar Energy Potential Atlas. (2025). https://gepa.enerji.gov.tr/pages/42.aspx
Göksu, T. T. (2024). Energy, exergy analysis, and RSM modeling of different designed twisted tapes in placed PV/T systems. *Energy*, *304*, 132041. https://doi.org/10.1016/J.ENERGY.2024.132041
Gomaa, M. R., Ahmed, M., & Rezk, H. (2022). Temperature distribution modeling of PV and cooling water PV/T collectors through thin and thick cooling cross-fined channel box. *Energy Reports*, *8*, 1144–1153. https://doi.org/10.1016/j.egyr.2021.11.061
K. S., U., Pathipati, S. B., & Bandaru, R. (2024). Analysis of Augmentation in Performance of Pv Module Integrated With Finned Pcm By Three-Dimensional Transient Numerical Simulation. *Isı Bilimi ve Tekniği Dergisi*, *44*(1), 143–162. https://doi.org/10.47480/isibted.1494403
Kaneria, P., & Reddy, K. S. (2025). *Minimizing shadow effects to optimize solar energy input in the World Solar Challenge*. *X*(X). https://doi.org/10.36922/GTI025090004
Karaaslan, I., & Menlik, T. (2021). Numerical study of a photovoltaic thermal (PV/T) system using mono and hybrid nanofluid. *Solar Energy*, *224*(March), 1260–1270. https://doi.org/10.1016/j.solener.2021.06.072
Kutlu, C., Erdinc, M. T., Ehtiwesh, A., BOTTARELLI, M., SU, Y., & RIFFAT, S. (2025). Evaluation of operation control parameters of a residential solar organic Rankine cycle with effects of expander-generator coupling. *Global Decarbonisation Journal*, *1*, 1–19.
Lu, L., & Yang, H. X. (2010). Environmental payback time analysis of a roof-mounted building-integrated photovoltaic (BIPV) system in Hong Kong. *Applied Energy*, *87*(12), 3625–3631. https://doi.org/10.1016/j.apenergy.2010.06.011
Peng, J., Lu, L., & Yang, H. (2013). Review on life cycle assessment of energy payback and greenhouse gas emission of solar photovoltaic systems. *Renewable and Sustainable Energy Reviews*, *19*, 255–274. https://doi.org/10.1016/j.rser.2012.11.035
Prasetyo, S. D., Arifin, Z., Prabowo, A. R., & Budiana, E. P. (2024). Investigation of the addition of fins in the collector of water/Al2O3-based PV/T system: Validation of 3D CFD with experimental study. *Case Studies in Thermal Engineering*, *60*(March), 104682. https://doi.org/10.1016/j.csite.2024.104682
Prasetyo, S. D., Budiana, E. P., Prabowo, A. R., & Arifin, Z. (2023). Modeling Finned Thermal Collector Construction Nanofluid-based Al2O3 to Enhance Photovoltaic Performance. *Civil Engineering Journal (Iran)*, *9*(12), 2989–3007. https://doi.org/10.28991/CEJ-2023-09-12-03
Prasetyo, S. D., Budiana, E. P., Prabowo, A. R., & Arifin, Z. (2024). Investigation of Finned Collectors on Photovoltaic Thermal Collector Performance Using Computational Fluids Dynamics Study. *Lecture Notes in Mechanical Engineering*, 391–399. https://doi.org/10.1007/978-981-97-0106-3_62
Qing, L. Z., Rosli, M. A. M., Salimen, N., Rashid, A. H. A., & Herawan, S. G. (2025). Assessment of Photovoltaic Thermal Efficiency using Phase Change Material and Water-Channel Collector

with T-Fin Design. *Journal of Advanced Research in Fluid Mechanics and Thermal Sciences*, *125*(1), 75–93. https://doi.org/10.37934/arfmts.125.1.7593

Rachoutis, E., & Koubogiannis, D. (2016). Energy Payback Time of a Rooftop Photovoltaic System in Greece. *IOP Conference Series: Materials Science and Engineering*, *161*(1). https://doi.org/10.1088/1757-899X/161/1/012092

Rao, V. T., Sekhar, Y. R., Pandey, A. K., Said, Z., Prasad, D. M. R., Hossain, M. S., & Selvaraj, J. (2022). Thermal analysis of hybrid photovoltaic-thermal water collector modified with latent heat thermal energy storage and two side serpentine absorber design. *Journal of Energy Storage*, *56*(PA), 105968. https://doi.org/10.1016/j.est.2022.105968

RefractiveIndex.INFO - Refractive index database. (n.d.). Retrieved March 25, 2025, from https://refractiveindex.info/

Smith, B. L., Sekar, A., Mirletz, H., Heath, G., & Margolis, R. (2024). *An Updated Life Cycle Assessment of Utility-Scale Solar Photovoltaic Systems Installed in the United States*. *March*, 85. www.nrel.gov/publications.

Souissi, A. S. E., Masmali, M., Fterich, M., Toutti, E., & Chouikhi, H. (2024). 3D Numerical Study and Parametric Analysis of PV/T Design Effect on Thermal and Electrical Performance. *Engineering, Technology and Applied Science Research*, *14*(3), 14175–14182. https://doi.org/10.48084/etasr.7227

Suman, S., Kaiser, J., Wei, S., & Wenbin, P. (2025). Assessing the Energy-Saving Potential of Passive Strategies in Commercial Buildings in the Top Upcoming Megacities. *Energy Catalyst*, *01*(1), 1–21. https://doi.org/10.61552/EC.2025.01.001

Tiwari, A., Raman, V., & Tiwari, G. N. (2007). Embodied energy analysis of hybrid photovoltaic thermal (PV/T) water collector. *International Journal of Ambient Energy*, *28*(4), 181–188. https://doi.org/10.1080/01430750.2007.9675042

Tonui, J. K., & Tripanagnostopoulos, Y. (2007). Improved PV/T solar collectors with heat extraction by forced or natural air circulation. *Renewable Energy*, *32*(4), 623–637. https://doi.org/10.1016/j.renene.2006.03.006

Unnikrishnan, K. S., Santhosh, K., & Rohinikumar, B. (2024). Experimental and numerical analysis of PV-PCM integrated with novel shaped corrugated fins. *Thermal Science and Engineering Progress*, *50*(March), 102562. https://doi.org/10.1016/j.tsep.2024.102562

Yang, T., & Athienitis, A. K. (2012). A study of design options for a building integrated photovoltaic/thermal (BIPV/T) system with glazed air collector and multiple inlets. *Energy Procedia*, *30*, 177–186. https://doi.org/10.1016/j.egypro.2012.11.022

Zhong, S., Rakhe, P., & Pearce, J. M. (2017). Energy payback time of a solar photovoltaic powered waste plastic recyclebot system. *Recycling*, *2*(2), 1–16. https://doi.org/10.3390/recycling2020010